Acta Crystallographica Section B
Structural Science
ISSN 0108-7681

Structural chemistry of A_2MX_4 compounds (X = O, F) with isolated tetrahedral anions: search for the densest structure types

Vladimir Nalbandyan* and Anastasiya Novikova

Chemistry Faculty, Southern Federal University, 7 ul. Zorge, Rostov-na-Donu 344090, Russian Federation

Correspondence e-mail: vbn@sfedu.ru

Received 6 August 2011
Accepted 1 April 2012

The packing density of various structures is important not only for understanding and the prediction of high-pressure phase transitions, but also because of its reported correlation with thermodynamic stability. Plotting the cube root of formula volume against the cation radii (R) for nine morphotropic series with isolated tetrahedral anions, A_2MO_4 (M = Si, Ge, S, Se, Cr, Mn, Mo, W) and A_2BeF_4, permits the comparison of packing densities for 13 structure types (about 80 individual compounds and several solid solutions) stable at (or near) ambient temperature. The spinel type is the densest. The next densest types are those of K_2MoO_4, Tl_2CrO_4, β-Ca_2SiO_4, β-K_2SO_4, Ag_2CrO_4 and Sr_2GeO_4. In three series (M = Ge, Mo, W) the densest type comes with somewhat intermediate values of R, and not the largest, in contrast to the classical homology rule. Another contradiction with traditional views is that some of the densest phases have abnormally low overall binding energies. The correlation between packing density and coordination number (CN) is better when CN of A counts entire MX_4 groups rather than individual X atoms; many, but not all, A_2MX_4 structures have binary A_2M analogues (of course, A and M are not necessarily the same in these structure types). The most frequent arrangement of A around M is of the Ni_2In type: a (distorted) pentacapped trigonal prism.

1. Introduction

Packing density is one of the most important structural characteristics of a condensed phase. It is of major interest as it is connected with the problem of high-pressure phase transitions which play a large role in both geophysics and materials science (Prewitt & Downs, 1998; McMillan, 2003; Manjon & Errandonea, 2009; Brazhkin, 2007; Demazeau, 2008). However, packing density is also important in the more general context of structural chemistry because of its direct correlation with the thermodynamic stability of various phases (Jenkins *et al.*, 1999, 2002; Glasser & Jenkins, 2000; Jenkins & Glasser, 2006). Higher packing density (hence a lower formula volume) means shorter bond lengths and/or higher coordination numbers (CNs). Therefore, it seemed obvious at the beginning of this work that this should provide stronger bonding and higher thermodynamic stability, at least at low temperatures and when high density is intrinsic and not a result of an external pressure. This is the classical principle of maximum space filling (Vainstein *et al.*, 1979). However, this was not confirmed by analysis of the experimental data (see §3.4).

There is a classical 'homology rule' supported by a great number of experimental data. It claims that elements behave at high pressures like heavier elements of the same group of

Table 1
Examples of correlations between formula volumes V/Z and ionic sizes: five variants of least-squares fits.

CR and IR are octahedral 'crystal' and 'ionic' radii (Shannon, 1976), R_0 is the bond-valence parameter (Brown & Altermatt, 1985; O'Keeffe & Brese, 1991) and φ^2 is the correlation factor (the conventional symbol R^2 was changed to avoid confusion with ionic radius). Maximum φ^2 in each line is highlighted in bold type.

Structure type	Formula type	Range of R (Å)	Number of points	φ^2				
				$(V/Z)^{1/3}$ *versus* R_0	V/Z *versus* $(IR)^3$	V/Z *versus* CR	V/Z *versus* $(CR)^3$	$(V/Z)^{1/3}$ *versus* CR
Rock salt	*A*F (Kabekkodu, 2007)	0.90–1.81 (*A* = Li . . . Cs)	5	**0.9991**	0.9934	0.9867	0.9957	0.9989
Rock salt	*A*O (Kabekkodu, 2007)	0.83–1.49 (*A* = Ni . . . Ba)	11	0.997	0.9882	0.9915	0.9924	**0.9989**
Delafossite	$Cu^{+}MO_2$ (Marquardt *et al.*, 2006)	0.675–1.172 (*M* = Al . . . La)	14	0.9907	0.9945	0.9945	0.9968	**0.9987**
Ilmenite	$A^{+}SbO_3$ (Nalbandyan *et al.*, 2006)	0.90–1.66 (*A* = Li . . . Rb)	5	0.984	0.9884	0.9920	0.9920	**0.9970**
Perovskite	$CaMO_3$ (Kabekkodu, 2007)	0.67–0.915 (*M* = Mn . . . Pb)	15	0.9353	0.9858	0.9895	0.9890	**0.9906**
Perovskite	$A^{3+}FeO_3$ (Kabekkodu, 2007)	1.001–1.172 (*M* = Lu . . . La)	15	0.9735	0.9942	**0.9977**	0.9949	0.9975
Perovskite	$A^{2+}TiO_3$ (Kabekkodu, 2007)	1.09–1.49 (*A* = Cd . . . Ba)	5	0.9916	0.9984	0.9915	**0.9987**	0.9942
Antifluorite	A_2O (Kabekkodu, 2007)	0.90–1.66 (*A* = Li . . . Rb)	4	0.9993	0.974	**0.9998**	0.9788	0.9891
Fluorite	AF_2 (Kabekkodu, 2007)	1.09–1.49 (*A* = Cd . . . Ba)	9	0.9528	0.9749	**0.9747**	0.9719	0.9742
Average				0.9804	0.9880	0.9909	0.9900	**0.9932**

the periodic table at lower pressures (Joubert & Chenavas, 1979; Vereschagin & Kabalkina, 1979; Sharma & Sikka, 1995; Prewitt & Downs, 1998; Orosel *et al.*, 2005; Vegas, 2011).

We must, however, distinguish between several entirely different cases. For elemental solids, where all the atoms are of the same size, geometrical relations are of no use and the main factor determining the increase in CN and in packing density is the change in *atomic* properties from non-metallic to metallic, best illustrated by the sequence C, Si, Ge, Sn, Pb. On the other hand, for binary compounds of ionic or iono-covalent nature, the radius ratio plays a major role. In this context, 'heavier' actually means 'having a larger atomic or ionic radius' (Vereschagin & Kabalkina, 1979). Since electropositive components ('cations' for short) are usually smaller than 'anions', both in size and in number, the CN is usually limited by anion–anion repulsion around a cation. Then the cation radius increase indeed favours larger CN and denser packing. However, the situation changes to the opposite with very large univalent cations. Well known (although rare) examples where the increase in cation-to-anion radius ratio leads to *less* dense structures with lower CNs are transitions from CsCl (CN 8–8) to CsF (CN 6–6) and from Rb_2O (CN 4–8) to Cs_2O (CN 3–6).

With ternary and more complex compositions, the situation becomes even less clear. One of the present authors has shown that substitution of a larger cation with an even larger one in several groups of mixed oxides systematically results in less dense structures (Nalbandyan *et al.*, 1979, 1995; Nalbandyan, 1986; Nalbandyan & Shukaev, 1987), although substitutions in the sublattices of smaller cations are in complete accordance with the classical homology rule. All these studies were limited to extended structures: three-dimensional frameworks and two-dimensional layered phases. Here, we start systematic studies of volume relations in structures with isolated anions. The first group under consideration is A_2MX_4 compounds with isolated tetrahedral anions where X = F or O. Although there are many papers reviewing the structural principles of A_2MX_4 or AM_2X_4 compounds (Kugimiya & Steinfink, 1968; Navrotsky, 1973, 1980, 1987; Lazoryak, 1996; Zakutkin & Blatov, 2001; Müller-Buschbaum, 2003; Ilyushin & Blatov, 2006; Zhang & Zunger, 2010; Blatov, 2011), most of them do not analyze volume relations at all or are concentrated on some specific high-pressure phase transitions, *e.g.* between phenacite, olivine and spinel types (Navrotsky, 1973, 1980, 1987). When this work was in progress, a book chapter appeared analyzing sequences of multiple phase transitions in the A_2MO_4 family (Vegas, 2011). However, it covers only part of the 13 structure types reviewed below and does not present the systematic analysis of correlations between ionic sizes, coordination numbers, packing densities and bonding energies.

2. Procedure

2.1. Method of comparison

How can we compare the packing densities of different structure types? The most direct way is to compare densities (or molar volumes or formula volumes V/Z) of different polymorphs having identical composition (here V is the unit-cell volume and Z is the number of formula units in the unit cell). Of course, this should be made under identical p–T conditions, and therefore only one of the forms may be thermodynamically stable, making this approach rarely applicable. A more general way is to build a morphotropic series, *i.e.* a group of compounds with identical general formulae and one variable component, to plot their characteristics against the size of that component and extrapolate the resulting graph for each structure type outside of its stability range. There are unambiguous relations between the density, molar volume and

formula volume of a compound, and between the radius and volume of a spherical ion. Therefore, the selection of the plot axes is merely a subject of convenience. For extrapolation purposes the graph should necessarily be linear. Thus, it is desirable that both argument and function be homogeneous in dimension, *e.g.* volume *versus* volume (Shannon, 1976) or length *versus* length (Nalbandyan *et al.*, 2006). We prefer the latter option because the absolute values of ionic radii are subject to a long dispute. Then the transition from one radii system to another (*e.g.* from Shannon's, 1976, *IR* to his *CR*) will change shapes of 'V/Z *versus* R^3' plots but will not change shapes of '$(V/Z)^{1/3}$ *versus* R' plots.

Of course, consideration of any specific structure demands using the CNs relevant for this structure (and for specific positions in it). However, for the comparison of different structures collectively, one needs a unified measure of ionic size independent of specific structures. We have chosen octahedral 'crystal' radii, tabulated by Shannon (1976) for all the A cations in question. Only for plots with fixed A and variable M we used the tetrahedral radii of M.

The applicability of this approach was tested on nine series of isotypic phases with wide ranges in ionic sizes. As evident from Table 1, '$(V/Z)^{1/3}$ *versus* R' plots (the last column) provide the best linearity whereas the bond-valence parameter, R_0, is the worst choice. It should be noted that for the last four series in the table, the actual CNs of the variable ions are different from six (for which the ionic radii were taken); moreover, the CNs of A vary in the perovskite structure from 8 to 12, together with a variation of the crystal system (orthorhombic, cubic and tetragonal). Nevertheless, the correlation factors are reasonably high even in these four series, *i.e.* the data satisfy linear relationships.

2.2. Data mining and selection

An extensive search has been performed using http://scholar.google.com, http://www.scopus.com and PDF-2 (Powder Diffraction File; Kabekkodu, 2007) which includes the complete data set imported from the Inorganic Crystal Structure Database (ICSD) and also a large number of entries with known unit cells and structure types not represented within the ICSD. Most data have then been verified using the original publications or at least their abstracts. This was necessary because information in the databases might miss important details or even be incorrect. For example, Cs_2MoO_4 was reported to be isostructural with β-K_2SO_4, but with the non-standard *Pcmn* setting of the space group 62 (Gonschorek & Hahn, 1973). In the databases the symbol was changed for the standard one, *Pnma*, but lattice constants were not interchanged. This resulted in an apparently 'new' structure type. Interestingly enough, this erroneous structure seemed rather realistic, with normal CNs, bond lengths and angles. Only too short a Cs—Cs distance of 2.77 Å and disagreement between

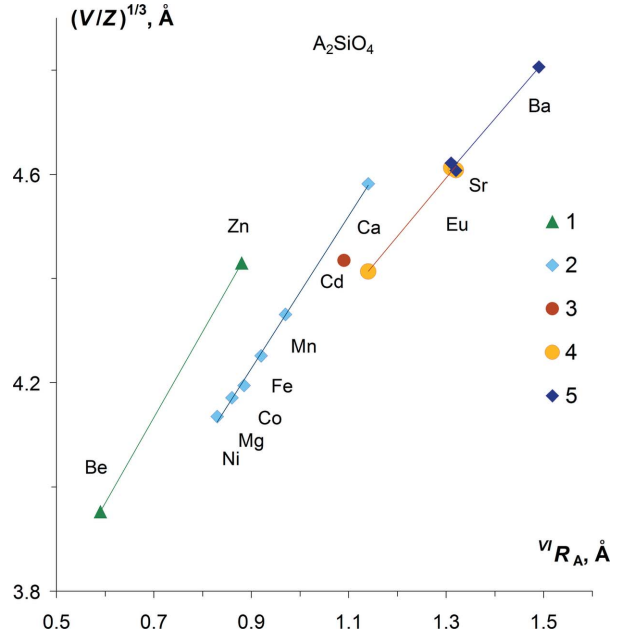

Figure 1
A plot of reduced cell parameters for A_2SiO_4 *versus* octahedral A^{2+} radii: 1, phenacite type for A = Be, Zn (Zachariasen, 1971; Hartman, 1989); 2, olivine type for A = Ni, Mg, Co, Fe, Mn, Ca (Tamada *et al.*, 1983; Yamazaki & Toraya, 1999; Fujino *et al.*, 1981; Mumme *et al.*, 1996); 3, thenardite type Cd_2SiO_4 (Dent-Glasser & Glasser, 1964); 4, larnite type (β-Ca_2SiO_4) for A = Ca, Eu, Sr (Jost *et al.*, 1977; Felsche, 1971; Catti, Gazzoni & Ivaldi, 1983); 5, β-K_2SO_4 type for A = Eu, Sr, Ba (Marchand *et al.*, 1978; Catti, Gazzoni, Ivaldi & Zanini, 1983; PDF 39-1256, Klockow & Eysel 1988; ICSD 6246, Grosse & Tillmanns, 1974).

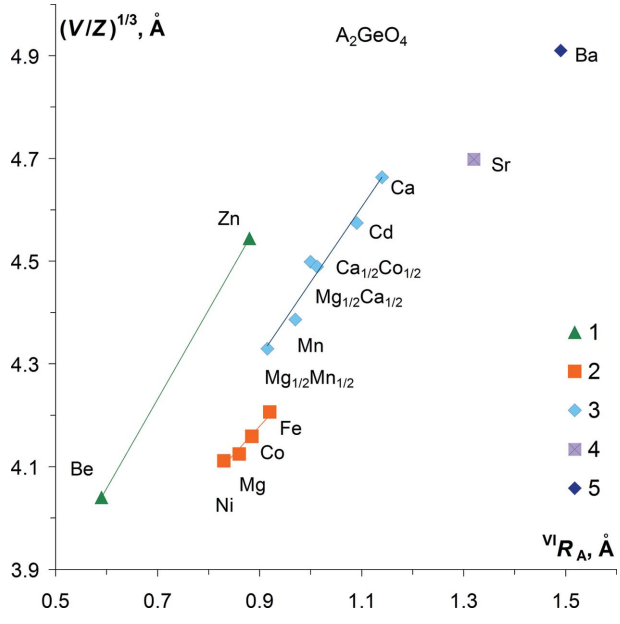

Figure 2
A plot of reduced cell parameters for A_2GeO_4 *versus* octahedral A^{2+} radii: 1, phenacite type for A = Be, Zn (PDF 10-83, Natl. Bur. Stand. (U.S.), 1960; Hang *et al.*, 1970); 2, spinel type for A = Ni, Mg, Co, Fe (Hirota *et al.*, 1990; Von Dreele & Navrotsky, 1977; Furuhashi *et al.*, 1973; Welch *et al.*, 2001); 3, olivine type for A = Mn, Cd, Ca (Creer & Troup, 1970; Simonov *et al.*, 1981; Eysel & Hahn, 1970), $MgMnGeO_4$ (ICSD 72908; Nord & Werner, 1992), $CaMgGeO_4$ (van Duijn *et al.*, 1995), and $CaCoGeO_4$ (PDF 36-1484; McMurdie *et al.*, 1986); 4, Sr_2GeO_4 (Nishi & Takeuchi, 1996); 5, β-K_2SO_4 type Ba_2GeO_4 (PDF 39-1257; Klockow & Eysel, 1988).

the calculated and experimental powder diffraction patterns might be signs of this error.

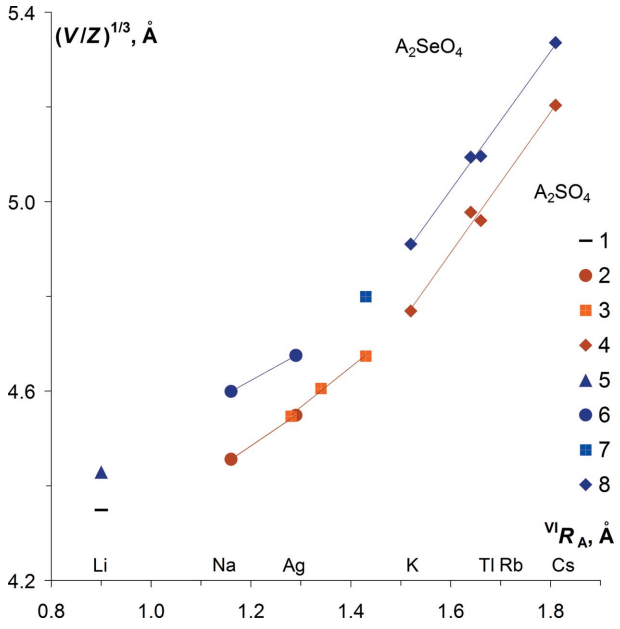

Figure 3
Plots of reduced cell parameters for A_2SO_4 (1–4) and A_2SeO_4 (5–8) *versus* octahedral A^+ radii: 1, Li_2SO_4 (Nord, 1976); 2 and 6, thenardite type for A = Na, Ag (Nord, 1973; ICSD 27655; Mehrotra *et al.*, 1978; Kálmán & Cruickshank, 1970; Weil, 2003); 3 and 7, glaserite type $K_{2/3}Na_{4/3}SO_4$ [PDF 20-926, Natl. Bur. Stand. (U.S.), 1968], $KNaSO_4$ and $K_{3/2}Na_{1/2}SO_4$ (Okada & Ossaka, 1980), $K_{3/2}Na_{1/2}SeO_4$ (PDF 26-923; Mehrotra, 1973); 4 and 8, β-K_2SO_4 type for A = K, Tl, Rb, Cs (McGinnety, 1972; Pannetier & Gaultier, 1966; Weber *et al.*, 1989; Gonzalez-Silgo *et al.*, 1996; Fábry & Breczewski, 1993; Takahashi *et al.*, 1987; Zúñiga *et al.*, 1991); 5, phenacite-type Li_2SeO_4 (Hartman, 1989).

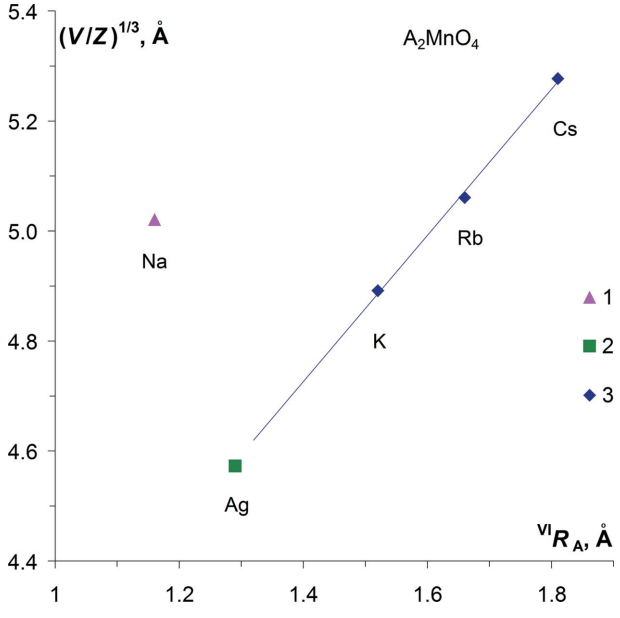

Figure 4
A plot of reduced cell parameters for A_2MnO_4 *versus* octahedral A^+ radii: 1, Na_2MnO_4 (Kopelev *et al.*, 1991); 2, Ag_2MnO_4 (Ag_2CrO_4 type; Chang & Jansen, 1983); 3, β-K_2SO_4 type for A = K, Rb, Cs (Kopelev *et al.*, 1991; Palenik, 1967; Fischer & Hoppe, 1995).

We found many dozens of different phases, selected only those stable at (or near) ambient conditions, identified their structure types and plotted their reduced unit-cell parameters, $(V/Z)^{1/3}$, against an ionic radii of A or M.

With X = F in A_2MX_4, M should be divalent, the only divalent metal forming stable tetrahedral fluorocomplexes being beryllium. With X = O, M should be either tetravalent (Si or Ge) or hexavalent (S, Se, Cr, Mn, Mo and W). In the A_2MO_4 series with these eight M elements, all compounds stable at normal T–p conditions contain only tetrahedral anions although some of them may change CN at high pressures. Not included (and will be analyzed elsewhere) are those series where only part of the compound is tetrahedral, *e.g.* A_2RuO_4, tetrahedral with A = K, Rb, Cs (Fischer & Hoppe, 1990; Fischer *et al.*, 2005) but based on pentacoordinate Ru with A = Na (Mogare *et al.*, 2004).

Mixed-cation $(A,A')_2MO_4$ phases with crystal structures different from those of the ternary components are not considered here. The only exception is the glaserite (or aphthitalite) type with the ideal formula $K_3Na(SO_4)_2$. This is based on extensive cationic substitutions (*e.g.* up to $KNaSO_4$ composition) and on the existence of *ternary* glaserite-type phases, Tl_2WO_4 (Okada *et al.*, 1979) and Tl_2MoO_4 (Friese *et al.*, 2001), although the latter exhibits slight monoclinic distortion at room temperature. Also included are solid

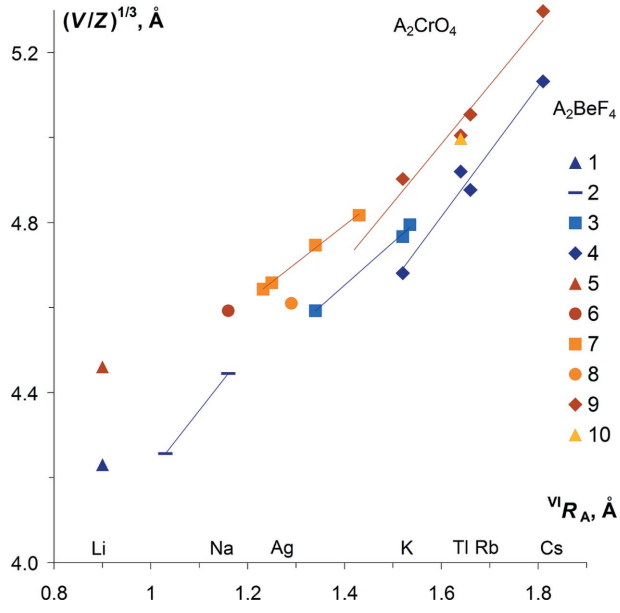

Figure 5
Plots of reduced cell parameters for A_2BeF_4 (1–4) and A_2CrO_4 (5–10) *versus* octahedral A^+ radii: 1 and 5, phenacite type for A = Li (Hartman, 1989; Brown & Faggiani, 1975); 2, olivine-type $LiNaBeF_4$ (Jahn, 1954) and Na_2BeF_4 (Deganello, 1972); 3 and 7, glaserite-type $NaKBeF_4$, $NaTlBeF_4$ and $Na_{1/2}Rb_{3/2}BeF_4$ (Pontonnier *et al.*, 1972), $Na_{1.6}K_{0.4}CrO_4$ (PDF 26-1332, Goldberg *et al.*, 1973), $Na_{3/2}K_{1/2}CrO_4$ (PDF 26-1467; Goldberg *et al.*, 1973), $NaKCrO_4$ (PDF 26-1468; Goldberg *et al.*, 1973), $K_{3/2}Na_{1/2}CrO_4$ (Madariaga & Breczewski, 1990); 4 and 9, β-K_2SO_4 type for A = K, Tl, Rb, Cs (McGinnety, 1972; da Silva *et al.*, 2005*a*,*b*; Carter & Margulis, 1972; Aleksovska *et al.*, 1998; ICSD 300021; Morris *et al.*, 1981); 6, Na_2CrO_4 (Nimmo, 1981); 8, Ag_2CrO_4 (Hackert & Jacobson, 1971); 10, Tl_2CrO_4 (Fábry *et al.*, 2010).

solutions which enable extending the stability ranges of structures in terms of radii. In all these cases we used the arithmetic mean radii based on actual cation fractions.

3. Results and discussion

3.1. Comparison of packing densities

The plots of reduced cell parameters *versus* ionic radii are shown in Figs. 1–9. Approximately 80 individual compounds and several solid solutions stable at (or near) ambient temperature have been identified in the nine morphotropic series investigated (actually there are seven additional series with fixed A and variable M, Figs. 8 and 9). They belong to 14 different structure types listed in Table 2 and illustrated in Fig. 10. Interestingly enough, there are three different structure types with the identical space group *Pnma*, two different structure types with the space group $P2_1/a$ ($P2_1/n$ in another setting) and two more with the space group $C2/m$. The β-K_2SO_4 type is the most populous, including 33% of all the compounds studied, whereas six other types are rare, represented by only one or two compounds. However, they may have isomorphs in different morphotropic series and/or at non-ambient conditions. *e.g.* the 'unique' structure of Na_2CrO_4 (*Cmcm*) is repeated in Na_2SO_4 at elevated temperatures (Tanaka *et al.*, 1991), in Na_2FeO_4 (Malchus & Jansen, 1998) and various $A^+A^{2+}MO_4$ (M = V, P; Paques-Ledent, 1975; Ijdo, 1982; Sato & Kano, 1994; Hata & Marumo, 1982) at ambient conditions.

The case of Na_2MnO_4 (Kopelev *et al.*, 1991) seems very strange (see Figs. 4 and 9). Based on an unpublished powder

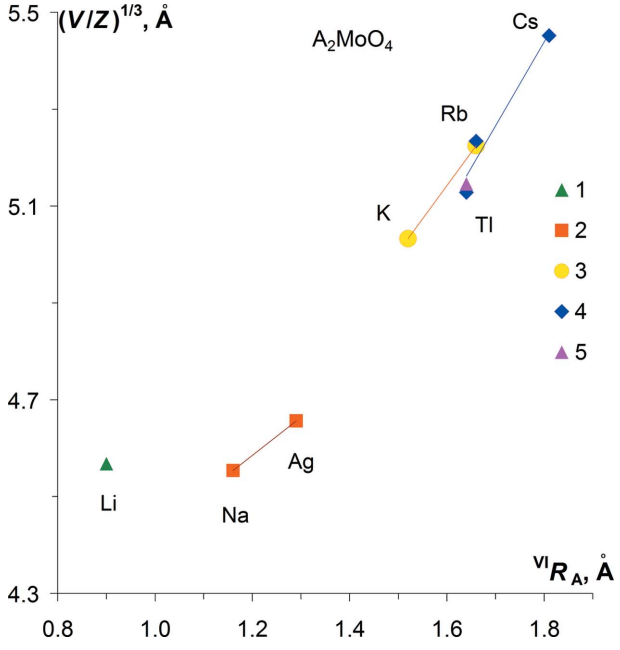

Figure 6
A plot of reduced cell parameters for A_2MoO_4 *versus* octahedral A^+ radii: 1, phenacite-type Li_2MoO_4 (Kolitsch, 2001); 2, spinel type for A = Na, Ag [Lindqvist, 1950; PDF 8-473, Natl. Bur. Stand. (U.S.), 1957]; 3, K_2MoO_4 type for A = K, Rb (Gatehouse & Leverett, 1969; Kools *et al.*, 1970); 4, β-K_2SO_4 type for A = Tl, Rb, Cs (Gonschorek & Hahn, 1973; Kools *et al.*, 1970; Shigematsu *et al.*, 2011; PDF 29-1341; Gaultier & Pannetier, 1972); 5, distorted glaserite-type Tl_2MoO_4 (Friese *et al.*, 2001).

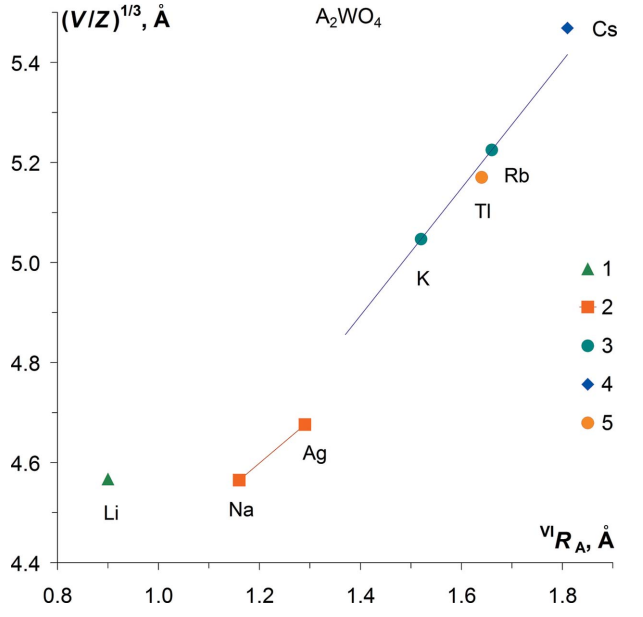

Figure 7
A plot of reduced cell parameters for A_2WO_4 *versus* octahedral A^+ radii: 1, phenacite-type Li_2WO_4 (Hartman, 1989); 2, spinel type for A = Na, Ag (Okada *et al.*, 1974; van den Berg & Juffermans, 1982); 3, K_2MoO_4 type for A = K, Rb (Kools *et al.*, 1970; Shigematsu *et al.*, 2011); 4, β-K_2SO_4 type Cs_2WO_4 (Kools *et al.*, 1970); 5, glaserite-type Tl_2WO_4 (Okada *et al.*, 1979).

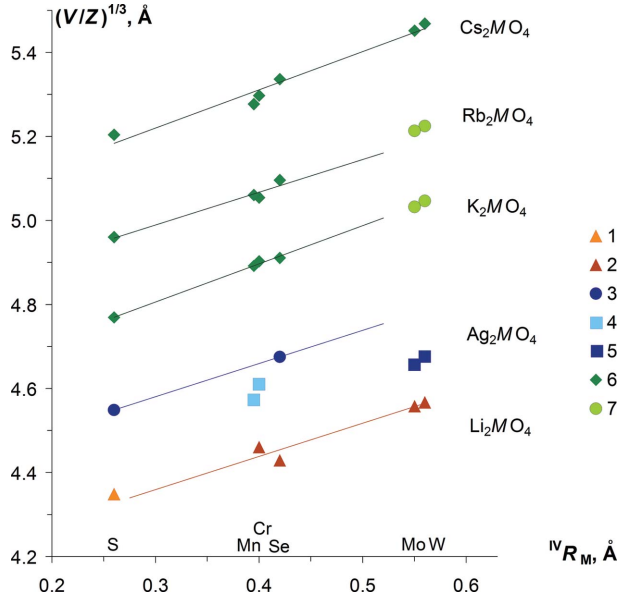

Figure 8
Plots of reduced cell parameters for Li_2MO_4, Ag_2MO_4, K_2MO_4, Rb_2MO_4 and Cs_2MO_4 *versus* tetrahedral M^{6+} radii: 1, Li_2SO_4; 2, phenacite type; 3, thenardite type; 4, Ag_2CrO_4 type; 5, spinel type; 6, β-K_2SO_4 type; 7, K_2MoO_4 type.

Table 2
Coordination numbers in A_2MO_4 and A_2BeF_4 structure types with isolated tetrahedral anions.

Where possible, the types are listed in ascending order of packing density according to Fig. 11. *N* is the number of individual compounds belonging to the given type within nine series under consideration. For definitions of CN1, CN2 and CN3, see §3.2.

			CN of *A*			Coordination of *M* with respect to *A* (see Fig. 10)			
Structure type	*N*	Space group	CN1	CN2	CN3	CN2	MA_n polyhedron with CN2	CN3	MA_n polyhedron with CN3
Phenacite	9	$R\bar{3}$ (148)	4	4	4	8	Strongly distorted bicapped trigonal prism	Same as CN2	
Li_2SO_4	1	$P2_1/a$ (14)	4	4	4	8	Distorted cube	Same as CN2	
Olivine	10	*Pnma* (62)	6, 6	4, 5	4, 5	9	Tricapped trigonal prism	Same as CN2	
Na_2MnO_4	1	$P6_3mc$ (186)	6, 4	6, 2	6, 5	8	Trigonal prism bicapped on triangular faces, Föppl symbol 1:3:3:1	11	Pentacapped trigonal prism
Thenardite	5	*Fddd* (70)	6	5	5	10	Planar hexagon combined with elongated tetrahedron, Föppl symbol 2:6:2	Same as CN2	
Glaserite	8	$P\bar{3}m1$ (164)	12, 10, 10, 6	6, 5	6, 5	11	Pentacapped trigonal prism	Same as CN2	
Na_2CrO_4	1	*Cmcm* (63)	4 + 2, 6	5, 6	5, 6	11	Pentacapped trigonal prism	Same as CN2	
Ag_2CrO_4	2	*Pnma* (62)	6, 4	6, 4	6, 5	10	Tetracapped trigonal prism	11	Pentacapped trigonal prism
Sr_2GeO_4	1	$Pbn2_1$ (33)	6, 8	5, 6	5, 6	11	Distorted pentacapped trigonal prism	Same as CN2	
β-K_2SO_4	27	*Pnma* (62)	10 + 1, 9	5, 6	5, 6	11	Distorted pentacapped trigonal prism	Same as CN2	
Larnite (β-Ca_2SiO_4)	3	$P2_1/n$ (14)	7, 8	5, 6	5, 6	11	Strongly distorted pentacapped trigonal prism	Same as CN2	
K_2MoO_4	4	*C*2/*m* (12)	8, 8	5, 6	5, 6	11	No common name; Föppl symbols 3:5:3 or 3:6:2	Same as CN2	
Tl_2CrO_4	1	*C*2/*m* (12)	8, 9, 9, 8	5, 6	5, 6	11	No common name; Föppl symbol 3:5:3	Same as CN2	
Spinel	8	$Fd\bar{3}m$ (227)	6	6	6	12	Laves tetrahedron	Same as CN2	

pattern, it was suggested to be isostructural with the high-temperature α-K_2SO_4. However, the reported unit-cell volume of the sodium compound at room temperature is 4% larger than that of α-K_2SO_4 at 847 K (Arnold *et al.*, 1981), which seems impossible. Na—O distances are unrealistically long: 2.77 Å × 6 for Na1 and 2.92 Å × 4 for Na2, whereas the corresponding normal values are 2.38 and 2.35 Å (Shannon, 1976). We conclude that the structure and/or composition of the compound might be erroneous and do not consider these data further.

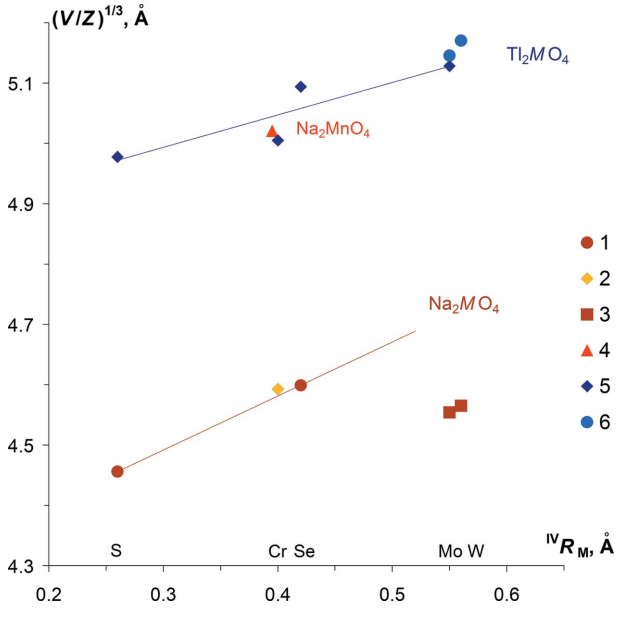

Figure 9
Plots of reduced cell parameters for Na_2MO_4 (1–4) and Tl_2MO_4 (5–6) *versus* tetrahedral M^{6+} radii: 1, thenardite type for *M* = S, Se; 2, Na_2CrO_4; 3, spinel type for *M* = Mo, W; 4, Na_2MnO_4; 5, β-K_2SO_4 type for *M* = S, Se, Cr, Mo; 6, glaserite type for *M* = Mo, W.

Very large volume differences between phenacite, olivine and spinel are well known (Navrotsky, 1973, 1980, 1987), but many other differences are small and need careful examination. The four monoclinic phases: Tl_2CrO_4 (Fábry *et al.*, 2010), larnite-type A_2SiO_4 where *A* = Sr, Eu (Catti, Gazzoni & Ivaldi, 1983; Felsche, 1971) and Rb_2MoO_4 (K_2MoO_4 type, Kools *et al.*, 1970) are denser than their orthorhombic β-K_2SO_4-type polymorphs by 0.4, 0.6, 0.6 and 1.0%, respectively. The difference between structure types of β-K_2SO_4 and K_2MoO_4 is also evident from the plot for A_2WO_4 compounds (Fig. 7), although the plot for K_2MO_4 (Fig. 8) does not show any volume drop between these types. Besides, larnite-type Sr_2GeO_4 (PDF 71-5095; Nishi & Takeuchi, 1991) is 0.4% denser than the stable $Pbn2_1$ polymorph (Nishi & Takeuchi, 1996). These data suggest that β-K_2SO_4 and Sr_2GeO_4 ($Pbn2_1$) types have essentially identical packing density, whereas the packing density of Tl_2CrO_4, larnite and K_2MoO_4 types is slightly higher and, again, almost the same for the three types.

Similarly, comparing the formula volumes of the *Fddd* and *Cmcm* polymorphs of Na_2SO_4 (Nord, 1973; Tanaka *et al.*, 1991) shows that the high-temperature phase, isostructural with Na_2CrO_4, is ∼ 1% denser, although the plot for Na_2MO_4 (Fig. 9) does not support this trend. Obviously, these very small differences may be partially due to experimental uncertainties; they may disappear or even change their sign in

different compounds and/or under different p–T conditions because of variations in thermal expansion and compressibility. Nevertheless, they predict the proper direction for some high-pressure transitions (see §3.3).

The estimation of other volume differences is based on the extrapolation or interpolation of plots for all series with variable A (Figs. 1–7) and variable M (Figs. 8 and 9) and, of course, is not so straightforward as with polymorphs. For example, we had to assume approximately equal packing density for Ag_2CrO_4 and β-K_2SO_4 (Figs. 4 and 5) types, thenardite and glaserite (Fig. 3), Na_2CrO_4 and glaserite (Fig. 5), but only within an accuracy limit of *ca* 1–2%.

Comparison of the glaserite and β-K_2SO_4 types might seem contradictory. However, the only indication that the glaserite type is slightly denser (Fig. 7) appears from comparison of Tl_2WO_4 with alkali compounds, whereas in cases where only Tl or only non-Tl compounds are compared (Figs. 5 and 9), the β-K_2SO_4 type is definitely denser. Therefore, the anomaly of Fig. 7 may be attributed to some specific features of the Tl^+ structural chemistry: the effect of its lone pair and/or low ionicity of the Tl—O bond.

The conclusions are summarized in Fig. 11, where packing density increases from top to bottom. The spinel type is the densest of all, and the least dense are those of Li_2SO_4 and phenacite.

3.2. Correlations between packing density, coordination numbers and ionic radii

Figs. 1–9 show that in most cases an increase in ionic radius gives rise to lower formula volumes, *i.e.* to denser structure types, in accordance with the classical homology rule. However, there are also three morphotropic series where the densest type, spinel, appears with A cations of somewhat intermediate size (Figs. 2, 6 and 7). All these cases are associated with the largest M(6+), molybdenum and tungsten, and the largest M(4+), germanium. We may speculate that the maximum packing density is achieved with the somewhat optimum value of the overall 'cation'/'anion' (A_2M/X_4) volume ratio: with smaller M (S, Be, Mn, Cr, Si, Se) the A cations should be large, whereas with larger M the A cations should be smaller. The same conclusion may be drawn from the Tl_2MO_4 series (Fig. 9) where large Tl^+ combined with large W(6+) produce slight volume expansion (although the Cs_2MO_4, Rb_2MO_4 and K_2MO_4 series do not support this trend). Further studies of different morphotropic series are necessary to validate this idea.

Another contradiction with the classical principles is the fact that conventional CNs (shown in Fig. 11 below the

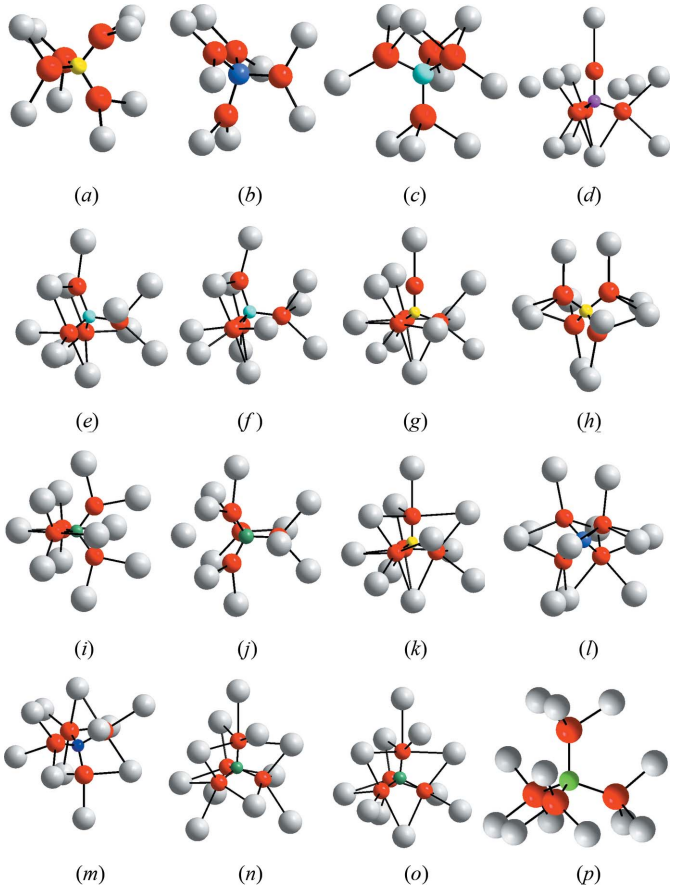

Figure 10
First and second coordination spheres of M atoms in A_2MO_4: (*a*) Li_2SO_4 (Nord, 1976); (*b*) phenacite-type Li_2BeF_4 (Collins *et al.*, 1983); (*c*) olivine Mg_2SiO_4 (Yamazaki & Toraya, 1999); (*d*) Na_2MnO_4 (α-K_2SO_4 type; Kopelev *et al.*, 1991); (*e*) and (*f*) Ge1 and Ge2 in Sr_2GeO_4 (Nishi & Takeuchi, 1996); (*g*) glaserite $K_3Na(SO_4)_2$ (Okada & Ossaka, 1980); (*h*) thenardite Na_2SO_4 (Nord, 1973); (*i*) Na_2CrO_4 (Nimmo, 1981); (*j*) Ag_2CrO_4 (Hackert & Jacobson, 1971); (*k*) β-K_2SO_4 (McGinnety, 1972); (*l*) K_2MoO_4 (Gatehouse & Leverett, 1969); (*m*) larnite β-Ca_2SiO_4 (Jost *et al.*, 1977); (*n*) and (*o*) Cr1*a* and Cr1*b* in Tl_2CrO_4 (Fábry *et al.*, 2010); (*p*) spinel-type Co_2GeO_4 (Furuhashi *et al.*, 1973).

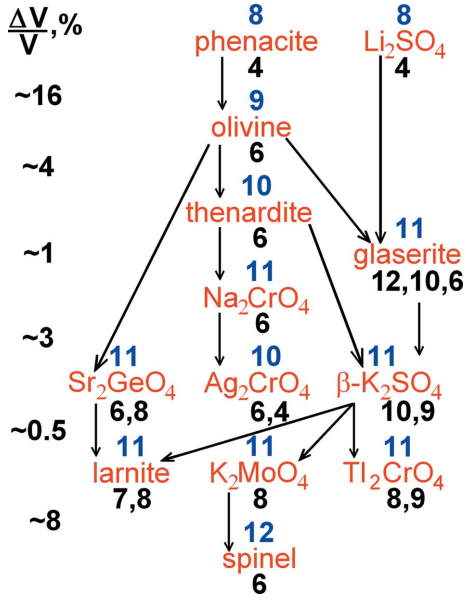

Figure 11
Comparison of packing densities of various A_2MX_4 types with isolated tetrahedra. Each arrow points to a denser type; types within a horizontal line have approximately equal packing densities; numbers above type names are CN2 of M (see Table 2) and numbers below type names are CN1 of A. Volume differences at the left column are only tentative because they vary with chemical composition.

designation of each type) in the denser structures are not necessarily larger. The most striking result is spinel again: with CN 6 of *A* it is denser than multiple structure types having CNs of 7–10, whereas the average CN of *A* varies from 5 to 9.5 in the six structure types with almost identical packing density. To clarify this situation, we suggest three different definitions of CN for *A* and *M*:

(i) CN1 is the conventional CN, *i.e.* number of *X* surrounding *A* or *M*;

(ii) CN2 is the number of electropositive atoms (*A* for *M* and *M* for *A*) bound to the given atom *via* common *X*;

(iii) CN3 is also the number of electropositive atoms of a different kind (*A* for *M* and *M* for *A*) surrounding the given atom within a sphere defined by the CN2, but not necessarily linked *via* common *X*. Usually, CN2 = CN3; however, there are two cases where CN3 is larger (see Table 2 and Fig. 10). Na_2CrO_4 may be the third case with CN2 of 3, 6 and 9, if we exclude the two longest Na—O contacts of 2.95 Å. In some Na_2CrO_4 isomorphs, these two contacts are actually non-bonding: *e.g.* in $LiMnVO_4$ (Sato & Kano, 1994), Li^+ has a tetrahedral environment with the fifth Li—O distance being 42% longer than the fourth.

CNs of *A* cations are often different within the same structure, whereas *M* positions are usually equivalent with two exceptions of Sr_2GeO_4 and Tl_2CrO_4 (Table 2, Fig. 10). Therefore, it is more convenient to discuss CN2 and CN3 of *M* which are obviously equal to sums of the corresponding CNs of the two *A* cations. Fig. 10 and Table 2 demonstrate that the most frequent CN2 and CN3 for *M* is 11, represented usually by a (distorted) pentacapped trigonal prism.

Examination of Fig. 11 shows that packing density correlates with CN2 much better than with CN1, with one exception of the transition from Na_2CrO_4 (CN2 = 11) to Ag_2CrO_4 (CN2 = 10). However, this contradiction is eliminated if CN3 is used, equal for both structures, or otherwise if fourfold coordination was adopted for Na1 leading to CN2 = 10 and CN3 = 11 for both structures. Therefore, the packing density of A_2MX_4 structures with isolated tetrahedra is much better determined by mutual coordination numbers of *A* and MX_4 (where MX_4 is considered as a single structureless particle) than by conventional atom-to-atom coordination numbers.

This approach immediately leads to the concept first introduced by O'Keeffe & Hyde (1985) and later developed by Vegas (2000, 2011), Vegas & Jansen (2002), Vegas & Mattesini (2010), Zakutkin & Blatov (2001), Ilyushin *et al.* (2004), Peskov & Blatov (2004, 2006) and Blatov (2011) emphasizing the analogy between mixed oxides and alloys: packing of 2*A* with isolated MX_4 is often analogous to that of a binary A_2M. Indeed, omitting oxygen or fluorine from the ideal spinel structure gives an ideal structure of the cubic Laves phases, *e.g.* $MgCu_2$; the thenardite type without O becomes similar to $TiSi_2$ having the same space group but with substantially different axial ratios; Li_2SO_4 ($P2_1/a$) shows some similarity with Li_2S antifluorite ($Fm3m$), although SLi_8 'cubes' in the former are strongly distorted; cationic arrangement of the Ni_2In type occurs not only in β-Ca_2SiO_4, Sr_2GeO_4, Na_2CrO_4, α- and β-K_2SO_4 (Blatov, 2011), but also in glaserite and Ag_2CrO_4 types. However, the relation between K_2SO_4 and cotunnite ($PbCl_2$), olivine and Ni_2In proposed by O'Keeffe & Hyde (1985) and Vegas (2011) is shown to be incorrect (Blatov, 2011): in both β- and α-K_2SO_4, the cationic environment of S is a pentacapped trigonal prism (Fig. 10), *i.e.* of the Ni_2In type, whereas the environment of Pb in cotunnite (Lumbreras *et al.*, 1986) consists of nine Cl in the form of a tricapped trigonal prism, with two additional 'caps' being Pb rather than Cl. The cationic environment of Si in olivine is also a distorted tricapped trigonal prism (Fig. 10*c*) where two additional caps are absent. Thus, olivine has no relation to Ni_2In or cotunnite. Monoclinic Tl_2CrO_4 is reported to be a slight distortion of the β-K_2SO_4-type polymorph. Indeed, $CrTl_{11}$ polyhedra of both polymorphs may be described by the Föppl symbol 3:5:3 as dictated by the mirror plane. Their shape, however, is changed significantly and both non-equivalent $CrTl_{11}$ groups of the monoclinic form do not resemble a pentacapped trigonal prism (1:3:3:3:1; Fig. 10).

We were not able to find binary compounds strictly analogous to phenacite, olivine, K_2MoO_4 and Tl_2CrO_4 types with their bizarre A_2M arrangements (Fig. 10 *b*, *c*, *l*, *n* and *o*).

Another analogy between complex and simple structures might be in the arrangement of the higher-valence atoms (here *M*) which often adopt 'close-packed' motifs or, more likely, eutaxy (O'Keeffe & Hyde, 1985). Indeed, in seven of the 13 structure types studied the *M* atoms were found to form a slightly distorted eutaxy: the 'three-layer' (cubic eutaxy) in Li_2SO_4 and 'two-layer' (hexagonal eutaxy) in all the types related to Ni_2In. There, each *M* has 12 nearest *M* neighbours with the shortest and longest *M*—*M* distances differing by 20–36%. Monoclinic Tl_2CrO_4 again represents an exclusion. Despite its claimed similarity to β-K_2SO_4, its 'eutaxy' is much more distorted, with the shortest and longest Cr—Cr distances differing by 65%. Moreover, one of the two independent Cr sites actually has a distorted cuboctahedral, rather than hexagonal, Cr_{12} environment. It is evident, however, that all these 'close-packed' *M* arrays have nothing to do with actual packing density: they appear in structures with low and intermediate packing densities, whereas the densest of the 12 structure types, spinel, has an *M* arrangement of the diamond type with CN of only four.

3.3. Prediction of high-pressure phase transformations

One of the goals of comparing packing densities was the prediction of phase transitions at high pressures. Note, however, that the arrows in Fig. 11 point to denser structure types but do not necessarily indicate the direction of the high-pressure phase transitions. The radius ratio of *A* and *M* also play a very important role in the stabilization of various structure types. In Fig. 11 structures of intermediate density (those of glaserite, β-K_2SO_4, K_2MoO_4 *etc.*) are characterized by large differences in the CNs and sizes of *A* and *M*, in contrast to structures in both the top and bottom of the diagram. Therefore, in any specific compound at increasing pressure, phase sequences such as 'fenacite-spinel' or 'olivine-spinel' are much more probable than 'fenacite-β-K_2SO_4-

spinel'. Compounds with a very large radius ratio of A and M, like Cs_2SO_4, are not expected to be spinels at any high pressure; for K_2WO_4 and K_2MoO_4, spinel phases are only slightly more probable.

Besides this the bond-valence principle should also be taken into account. In each of the six most populous monocationic structure types of Table 2 (β-K_2SO_4, olivine, fenacite, spinel, thenardite and K_2MoO_4), all O or F atoms have identical CNs with respect to A. On the other hand, in some rare types these CNs differ significantly, *e.g.* 4 and 2 in Na_2CrO_4, 3 and 2 in Ag_2CrO_4. Then, with equal bond lengths in each coordination group, the bond-valence sums for anions will deviate from the ideal values. With the formula type $A_2^+M^{6+}O_4$, the deviations are small and may be easily eliminated by slight changes in M—O bond lengths. However, with $A_2^{2+}M^{4+}O_4$ and A_2BeF_4 formula types, the relative deviations will be doubled and will destabilize the structures. Therefore, the structure types of Na_2CrO_4 and Ag_2CrO_4 will be less probable for silicates, germanates and fluoroberyllates.

An opposite trend is also evident (although not explained so far): none of the ten olivines and three larnites in Table 2 belong to the $A_2^+M^{6+}O_4$ formula type; therefore, olivine and larnite types are not appropriate for $A_2^+M^{6+}O_4$ compounds, at least at ambient conditions.

Having these considerations in mind, we tried to 'predict' possible high-pressure transformations on the basis of our plots, first ignoring the literature data, and then compared these 'predictions' with the experimental data in Table 3. The predictions, of course, could not be comprehensive, because Figs. 1–11 and Table 2 do not include many possible structure types, particularly those with octahedral M, which are much denser and thus preferable at high pressures. Nevertheless, Table 3 shows a reasonable fraction of correct predictions.

Only two predictions failed: new structure types not listed in Table 2 appeared as intermediate phases of Zn_2SiO_4 and decomposition products of Cd_2GeO_4.

Thirteen predictions have been confirmed with some deviations. These include the following cases:

(i) direct transitions from phenacite or olivine to spinel (or spinel-related) phases in seven cases, without the expected intermediate-density structures;

(ii) unrecognized intermediate phase in Li_2SO_4;

(iii) the appearance of spinel-related phases of lower symmetry instead of cubic spinels in Zn_2SiO_4, Li_2WO_4 and Mn_2GeO_4;

(iv) tentative indications of structure in Ca_2GeO_4 and Tl_2MoO_4.

Nine expected transitions (in Ca_2SiO_4, Li_2BeF_4, Sr_2SiO_4, Na_2SO_4, $AMnGeO_4$, where A = Mg, Co, Fe, and in A_2GeO_4, where A = Co, Ni) have been confirmed exactly, not to mention the cases where no transition was expected and no transition was observed up to very high pressures. As indicated above, we could not be in the firm belief concerning phase transitions between structure types having similar densities: thenardite to Na_2CrO_4 type in Na_2SO_4 and β-K_2SO_4 to larnite type in Sr_2SiO_4. However, they have been confirmed.

A strange example is represented by Rb_2SeO_4 (Ghedia, 2010). Its phase transition is not included in Table 3 because the high-pressure form has a 0.5% *larger* formula volume and yellow–green discolouration, indicating possible non-stoichiometry.

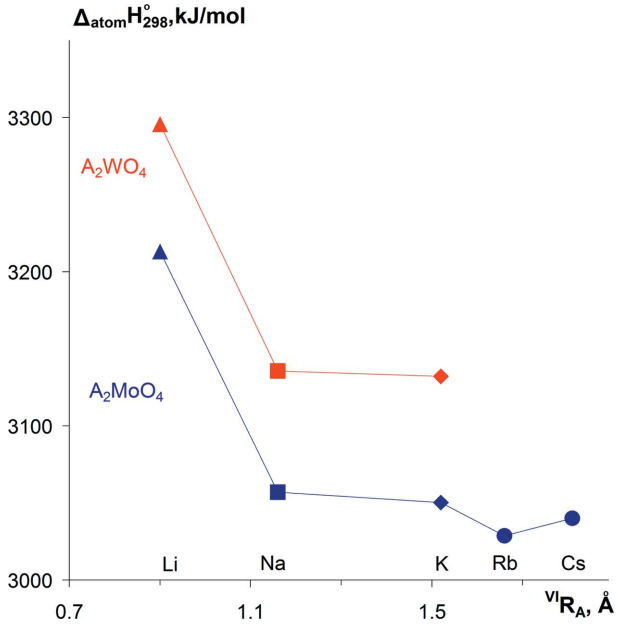

Figure 12
Standard heats of atomization of A_2MoO_4 and A_2WO_4 at 298.15 K *versus* ionic radii of A. Triangles, phenacites; squares, spinels; diamonds, K_2MoO_4 type; circles, β-K_2SO_4 type.

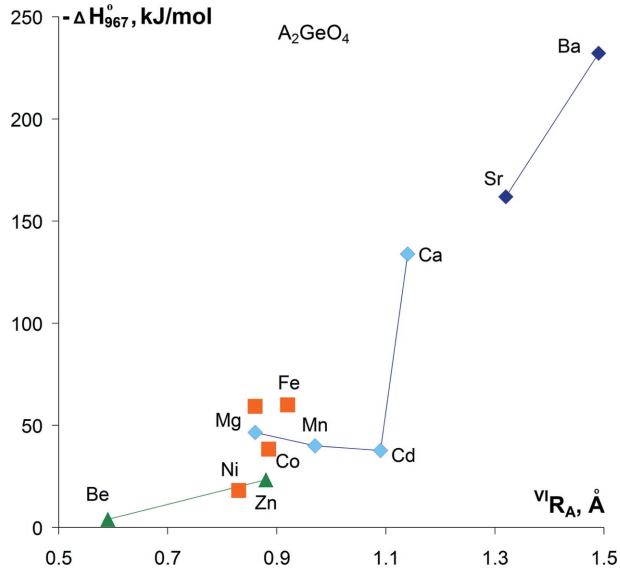

Figure 13
Standard heats of reactions $2AO + GeO_2$ (tetragonal) = A_2GeO_4 at 965 or 967 K (Navrotsky, 1971, 1987; Köther & Müller, 1978) *versus* ionic radii of A. Triangles, phenacites; squares, spinels; light diamonds, olivines; dark diamonds, β-K_2SO_4 type.

Table 3
Expected and observed sequences of low-temperature high-pressure (LT-HP) structure types for tetrahedral A_2MX_4 phases from Table 2.

In some instances, where no LT-HP transitions were reported or LT-HP amorphization was observed, high-temperature high-pressure (HT-HP) results are cited.

Compounds	Expected from Figs. 1–9 and 11	Observed experimentally
	According to the homology rule	
2 Zn_2MO_4, Li_2BeF_4	Olivine, then thenardite, then spinel	Zn_2SiO_4 (HT-HP): orthorhombic spinel-related with three intermediate not predicted phases (two of them being Zn-deficient)[a]; Zn_2GeO_4 (HT-HP)[a]: spinel; Li_2BeF_4: olivine[b]
Li_2SO_4 and 4 Li_2MO_4 phenacites	Thenardite, Na_2CrO_4 or Ag_2CrO_4, then spinel	Li_2MoO_4[c]: spinel; Li_2WO_4: tetragonal spinel-related[d]; Li_2SO_4: unrecognized phase, then Na_2CrO_4 type[e]; Li_2MO_4 (M = Cr, Se): unrecognized phase[f]
Cd_2SiO_4	Larnite	No transition up to 9.5 GPa[g]
4 $A_2^+M^{6+}O_4$ thenardites	Na_2CrO_4, then Ag_2CrO_4 or Sr_2GeO_4	Ag_2MO_4 (M = S, Se)[h], Na_2SeO_4[i]: no transitions up to 4 GPa; Na_2SO_4: Na_2CrO_4 type (Na_2SO_4-III), then unrecognized phase[j]
Na_2CrO_4	Ag_2CrO_4 or Sr_2GeO_4, then larnite or K_2MoO_4	Unrecognized phase[j]
2 Ag_2CrO_4-type	K_2MoO_4 or larnite, or Tl_2CrO_4, then spinel	Ag_2CrO_4: no transitions up to 4 GPa[h]; Ag_2MnO_4: no data found
Olivines with larger A/M radius ratio	Thenardite or Sr_2GeO_4 or larnite, then spinel	Na_2BeF_4: no transitions up to 3.5 GPa[b]; Ca_2SiO_4: larnite[k]; Cd_2GeO_4 (HT-HP): unrecognized phase, presumably tetrahedral, then CdO + $CdGeO_3$ perovskite[l]; Ca_2GeO_4: unrecognized phase, presumably larnite[m]; HT-HP: K_2NiF_4 type (octahedral)[l]; A_2SiO_4 (A = Ni, Mg, Co, Fe): spinel[n]; Mn_2SiO_4 (HT-HP): unrecognized phase, presumably tetrahedral[l] or MnO + $MnSiO_3$ (tetragonal garnet-related)[o]
	Unrelated to the homology rule	
3 larnites	Spinel or octahedral structures	Ca_2SiO_4: no transitions up to 24 GPa[k]; A_2SiO_4 (A = Sr, Eu): no data found
	Opposite to the homology rule	
Olivines with smaller A/M radius ratio	Spinel	$AMnGeO_4$ (A = Mg, Co, Fe): spinels (HT-HP)[p]; Mn_2GeO_4: modified spinel[k,q]
K_2MO_4 (M = Mo, W)	Spinel or octahedral structures	K_2MoO_4: no data found; K_2WO_4: unrecognized phase[r]
Sr_2GeO_4	Larnite, then spinel	No data found
19 β-K_2SO_4 phases with M = Mn, Si, Cr, Se, Ge, Mo, W	K_2MoO_4 or Tl_2CrO_4 or larnite; octahedral structures may appear at very high pressures	Sr_2SiO_4: larnite type[s]; K_2CrO_4: no transitions up to 52 GPa[t]; Tl_2SeO_4[u], K_2SeO_4[v]: no transitions up to 3.6–4.0 GPa; Cs_2SeO_4: no transitions up to 2.5 GPa[w]; Tl_2MoO_4: unrecognized phase, presumably with elevated CN of Mo[x]; other 13 compounds: no data found
8 β-K_2SO_4-type phases with M = S, Be	K_2MoO_4 or Tl_2CrO_4 or larnite	Cs_2SO_4: no transitions up to 16.4 GPa[y]; K_2SO_4: no transitions up to 4.0 GPa[v]; other 6 compounds: no data found
	No high-pressure tetrahedral structures predicted	
Be_2MO_4 (M = Si, Ge); 8 spinels; Rb_2MO_4 (M = Mo, W); Tl_2CrO_4	No tetrahedral structures of Table 2 are expected, but octahedral structures may appear at very high pressures	Be_2SiO_4: no transition up to 31 GPa[z]; Na_2MO_4 (M = Mo, W): no transitions up to 4.5 GPa[aa]; A_2GeO_4 (A = Ni, Co, Mg, Fe): no transitions up to 15 GPa, 1273 K[bb]; (A = Ni, Co): AO + GeO_2 (octahedral) at 25 GPa, 1673–2073 K[cc]; other six compounds: no data found

Note. 'Unrecognized phase' means that a phase transition was observed but XRD data were either not collected or not indexed definitely. This does not exclude formation of the expected structure. References: (*a*) Syono & Akimoto (1971), (*b*) Jackson (1977), (*c*) Liebertz & Rooymans (1967), (*d*) Horiuchi *et al.* (1979), (*e*) Parfitt *et al.* (2005), (*f*) Pistorius (1967*a*), (*g*) Miletich *et al.* (1998), (*h*) Pistorius (1967*b*), (*i*) Pistorius (1967*c*), (*j*) Pistorius (1967*d*), (*k*) Reynard *et al.* (1997), (*l*) Ringwood & Reid (1968), (*m*) Petit *et al.* (1996), (*n*) Navrotsky (1987), (*o*) Ito *et al.* (1974), (*p*) Ringwood & Reid (1970), (*q*) Morimoto *et al.* (1970), (*r*) Huang & Butler (1990), (*s*) Heindl *et al.* (1985), (*t*) Edwards *et al.* (1999), (*u*) Grzechnik *et al.* (2008), (*v*) Pistorius & Rapoport (1969), (*w*) Ethier *et al.* (1989), (*x*) Machon *et al.* (2010), (*y*) Ravindran & Arora (1999), (*z*) Fan *et al.* (2012), (*aa*) Pistorius (1966), (*bb*) Ringwood & Reid (1969), (*cc*) Liu (1976).

Note that most other predictions could not be verified due to insufficient experimental data. Thus, Table 3 leaves much space for further studies. Besides the transitions discussed, valence changes may be expected at high pressures in some compositions, *e.g.* $Tl_2^+Cr^{6+}O_4 \rightarrow Tl^+Tl^{3+}Cr^{4+}O_4 \rightarrow Tl_2^{3+}Cr^{2+}O_4$.

3.4. Search for correlation between packing density and binding energy

As mentioned in §1, it was expected initially that elevated packing density (if it is intrinsic and not forced by external pressure) should result in elevated binding energy. We tried to

verify this by comparison of thermochemical data for those three cases where the densest structure type appeared in the middle part of the morphotropic series.

For molybdates and tungstates, standard heats of atomization were calculated from their standard heats of formation (Glushko, 1982) and standard heats of atomization of the corresponding elements (Emsley, 1991) and plotted in Fig. 12. As might be expected, the overall binding energy decreases with increasing size of A but, unexpectedly, the Na_2MO_4 spinels in both series show considerable negative deviations from the general trend. A small negative deviation of Rb_2MoO_4 is due to the fact that the plotted value is that for its metastable orthorhombic form.

For germanates the necessary data for heats of atomization could not be found, and we could only plot their heats of formation from their corresponding oxides at high temperature. Of course, these data might be biased not only by experimental uncertainties (the values for A = Be, Mn, Fe were reported as rough estimates) but also by variations in characteristics of the starting binary oxides, crystal field stabilization energies of the 3*d* cations *etc.* This results in considerable scatter of the data (Fig. 13) and precludes definite conclusions.

For Mg_2GeO_4, however, the spinel-to-olivine transition is definitely endothermic (Navrotsky, 1987); therefore, the spinel form has higher binding energy. In this specific case the initial suggestion is confirmed but the data for Na_2MO_4 (M = Mo, W) seem to disprove it. In addition, quenched high-temperature forms of Na_2SO_4 and Sr_2GeO_4 are slightly denser than their stable polymorphs. It is not clear now whether these facts are due to experimental errors or the principle of maximum space filling should be modified (or even discredited). Further studies are planned to elucidate this point.

4. Conclusions

Among 13 tetrahedral A_2MX_4 structure types stable at ambient conditions, the densest is that of spinel and the six next densest, with packing densities equal within 1%, are those of K_2MoO_4, Tl_2CrO_4, β-Ca_2SiO_4, β-K_2SO_4, Ag_2CrO_4 and Sr_2GeO_4.

In contrast to the classical homology rule, maximum packing density is not necessarily associated with maximum cationic sizes; in the A_2MO_4 series where M = Mo, W or Ge, the densest structure type appears with A ions of intermediate size.

In contrast to the classical principle of maximum space filling, the densest phases may have reduced, rather than elevated, overall binding energies.

The correlation between packing density of A_2MX_4 and CN is better when CN of A counts entire MX_4 groups rather than individual X atoms.

A_2M subarrays in nine of the 13 structure types are similar to those in binary compounds: Ni_2In, $TiSi_2$, $MgCu_2$ or CaF_2.

The authors are thankful to anonymous reviewers whose useful comments stimulated major revision and addition of §§3.3 and 3.4.

References

Aleksovska, S., Nyburg, S. C., Pejov, Lj. & Petrusevski, V. M. (1998). *Acta Cryst.* B**54**, 115–120.
Arnold, H., Kurtz, W., Richter-Zlnnius, A., Bethke, J. & Heger, G. (1981). *Acta Cryst.* B**37**, 1643–1651.
Berg, A. J. van den & Juffermans, C. A. H. (1982). *J. Appl. Cryst.* **15**, 114–116.
Blatov, V. A. (2011). *Struct. Bond.* **138**, 31–66.
Brazhkin, V. V. (2007). *High Pressure Res.* **27**, 333–351.
Brown, I. D. & Altermatt, D. (1985). *Acta Cryst.* B**41**, 244–247.
Brown, I. D. & Faggiani, R. (1975). *Acta Cryst.* B**31**, 2364–2365.
Carter, R. L. & Margulis, T. N. (1972). *J. Solid State Chem.* **5**, 75–78.
Catti, M., Gazzoni, G. & Ivaldi, G. (1983). *Acta Cryst.* C**39**, 29–34.
Catti, M., Gazzoni, G., Ivaldi, G. & Zanini, G. (1983). *Acta Cryst.* B**39**, 674–679.
Chang, F. M. & Jansen, M. (1983). *Z. Anorg. Allg. Chem.* **507**, 59–65.
Collins, D. M., Mahar, M. C. & Whitehurst, F. W. (1983). *Acta Cryst.* B**39**, 303–306.
Creer, L. G. & Troup, G. J. F. (1970). *Solid State Commun.* **8**, 1183–1188.
Deganello, S. (1972). *Z. Kristallogr.* **135**, 18–33.
Demazeau, G. (2008). *High Pressure Res.* **28**, 483–489.
Dent-Glasser, L. S. & Glasser, F. P. (1964). *Inorg. Chem.* **3**, 1228–1230.
Duijn, J. van, de Graaf, R. A. G. & Ijdo, D. J. W. (1995). *Mater. Res. Bull.* **30**, 1489–1493.
Edwards, C. M., Haines, J., Butler, I. S. & Leger, J.-M. (1999). *J. Phys. Chem. Solids*, **60**, 529–538.
Emsley, J. (1991). *The Elements*. Oxford: Clarendon Press. (Russian Translation, Mir, 1993).
Ethier, L., Massa, N. E., Beliveau, A. & Carlone, C. (1989). *Can. J. Phys.* **67**, 657–663.
Eysel, W. & Hahn, T. (1970). *Z. Kristallogr.* **131**, 322–341.
Fábry, J. & Breczewski, T. (1993). *Acta Cryst.* C**49**, 1724–1727.
Fábry, J., Dušek, M., Fejfarová, K., Krupková, R. & Vaněk, P. (2010). *Acta Cryst.* C**66**, i45–i49.
Fan, D.-W., Ma, M.-N., Wei, S.-Y., Chen, Z.-Q. & Xie, H.-S. (2012). *Chin. Phys. C*, **36**, 179–183.
Felsche, J. (1971). *Naturwissenschaften*, **58**, 218–219.
Fischer, D. & Hoppe, R. (1990). *Z. Anorg. Allg. Chem.* **591**, 87–94.
Fischer, D. & Hoppe, R. (1995). *Z. Anorg. Allg. Chem.* **621**, 177–180.
Fischer, D., Hoppe, R., Mogare, K. M. & Jansen, M. (2005). *Z. Naturforsch. B*, **60**, 1113–1117.
Friese, K., Aroyo, M. I., Folcia, C. L., Madariaga, G. & Breczewski, T. (2001). *Acta Cryst.* B**57**, 142–150.
Fujino, K., Sasaki, S., Takéuchi, Y. & Sadanaga, R. (1981). *Acta Cryst.* B**37**, 513–518.
Furuhashi, H., Inagaki, M. & Naka, S. (1973). *J. Inorg. Nucl. Chem.* **35**, 3009–3014.
Gatehouse, B. M. & Leverett, P. (1969). *J. Chem. Soc. A*, pp. 849–854.
Gaultier, M. & Pannetier, G. (1972). *Rev. Chim. Miner.* **9**, 271–289. PDF 29-1341.
Ghedia, S. A. (2010). Dissertation. Universität Stuttgart, Germany.
Glasser, L. & Jenkins, H. D. B. (2000). *J. Am. Chem. Soc.* **122**, 632–638.
Glushko, V. P. (1982). Editor. *Termicheskie konstanty veschestv* (Thermal constants of substances), http://www.chem.msu.ru/cgi-bin/tkv.pl?show=welcome.html.
Goldberg, A., Eysel, W. & Hahn, T. (1973). *Neues Jahrb. Mineral. Monatsh.* **6**, 241. PDF 26-1332, 26-1467, 26-1468.
Gonschorek, W. & Hahn, T. H. (1973). *Z. Kristallogr.* **138**, 167–176.
Gonzalez-Silgo, C., Solans, X., Ruiz-Perez, C., Martinez-Sarrion, M. L. & Mestres, L. (1996). *Ferroelectrics*, **177**, 191–199.

Grosse, H. P. & Tillmanns, E. (1974). *Cryst. Struct. Commun.* **3**, 599–601. ICSD 6246.
Grzechnik, A., Breczewski, T. & Friese, K. (2008). *J. Solid State Chem.* **181**, 2914–2917.
Hackert, M. L. & Jacobson, R. A. (1971). *J. Solid State Chem.* **3**, 364–368.
Hang, C., Simonov, M. A. & Belov, N. V. (1970). *Kristallografiya*, **15**, 457–462 (in Russian).
Hartman, P. (1989). *Z. Kristallogr.* **187**, 139–143.
Hata, M. & Marumo, F. (1982). *Acta Cryst.* B**38**, 239–241.
Heindl, R., Amara, A., Tary, G., Loriers, J. & Lignou, F. (1985). *J. Mater. Sci. Lett.* **4**, 1449–1450.
Hirota, K., Inoue, T., Mochida, N. & Ohtsuka, A. (1990). *J. Ceram. Soc. Jpn*, **98**, 976–986.
Horiuchi, H., Morimoto, N. & Yamaoka, S. (1979). *J. Solid State Chem.* **30**, 129–135.
Huang, Y. & Butler, I. S. (1990). *Appl. Spectrosc.* **44**, 1326–1628.
IJdo, D. J. W. (1982). *Acta Cryst.* B**38**, 923–925.
Ilyushin, G. D. & Blatov, V. A. (2006). *Crystallogr. Rep.* **51**, 366–378.
Ilyushin, G. D., Blatov, V. A. & Zakutkin, Y. A. (2004). *Z. Kristallogr.* **219**, 468–478.
Ito, E., Matsumoto, T. & Kawai, N. (1974). *Phys. Earth Planet. Inter.* **8**, 241–245.
Jackson, I. (1977). *Phys. Earth Planet. Inter.* **14**, 143–164.
Jahn, W. (1954). *Z. Anorg. Allg. Chem.* **276**, 113–127.
Jenkins, H. D. & Glasser, L. (2006). *Inorg. Chem.* **45**, 1754–1756.
Jenkins, H. D., Roobottom, H. K., Passmore, J. & Glasser, L. (1999). *Inorg. Chem.* **38**, 3609–3620.
Jenkins, H. D., Tudela, D. & Glasser, L. (2002). *Inorg. Chem.* **41**, 2364–2367.
Jost, K. H., Ziemer, B. & Seydel, R. (1977). *Acta Cryst.* B**33**, 1696–1700.
Joubert, J. C. & Chenavas, J. (1979). *J. Solid State Chem.* **27**, 29–39.
Kabekkodu, S. (2007). Editor. *Powder Diffraction File*. International Centre for Diffraction Data, PA, USA.
Kálmán, A. & Cruickshank, D. W. J. (1970). *Acta Cryst.* B**26**, 436.
Klockow & Eysel, W. (1988). ICDD Grant-in-Aid. PDF 39-1256, 39-1257.
Kolitsch, U. (2001). *Z. Kristallogr.* **216**, 449–454.
Kools, F. X. N. M., Koster, A. S. & Rieck, G. D. (1970). *Acta Cryst.* B**26**, 1974–1977.
Kopelev, N. S., Val'kovskii, M. D., Popov, A. I. & Chumaevskii, N. A. (1991). *Zh. Neorg. Khim.* **36**, 2210–2216 (in Russian).
Köther, W. & Müller, F. (1978). *Z. Anorg. Allg. Chem.* **444**, 77–90.
Kugimiya, K. & Steinfink, H. (1968). *Inorg. Chem.* **7**, 1762–1770.
Lazoryak, B. I. (1996). *Russ. Chem. Rev.* **65**, 287–305.
Liebertz, J. & Rooymans, C. J. M. (1967). *Solid State Commun.* **5**, 405–409.
Lindqvist, I. (1950). *Acta Chem. Scand.* **4**, 1066–1074.
Liu, L.-G. (1976). *Earth Planet. Sci. Lett.* **31**, 393–396.
Lumbreras, M., Protas, J., Jebbari, S., Dirksen, G. J. & Schoonman, J. (1986). *Solid State Ionics*, **20**, 295–304.
Machon, D., Friese, K., Breczewski, T. & Grzechnik, A. (2010). *J. Solid State Chem.* **183**, 2558–2564.
Madariaga, G. & Breczewski, T. (1990). *Acta Cryst.* C**46**, 2019–2021.
Malchus, M. & Jansen, M. (1998). *Z. Anorg. Allg. Chem.* **624**, 1846–1854.
Manjon, F. J. & Errandonea, D. (2009). *Phys. Status Solidi B*, **246**, 9–31.
Marchand, R., L'Haridon, P. & Laurent, Y. (1978). *J. Solid State Chem.* **24**, 71–76.
Marquardt, M. A., Ashmore, N. A. & Cann, D. P. (2006). *Thin Solid Films*, **496**, 146–156.
McGinnety, J. A. (1972). *Acta Cryst.* B**28**, 2845–2852.
McMillan, P. F. (2003). *Chem. Commun.* pp. 919–923.
Mehrotra, B. N. (1973). ICDD Grant-in-Aid. PDF 26-923.
Mehrotra, B. N., Hahn, T., Eysel, W., Roepke, H. & Illguth, A. (1978). *Neues Jahrb. Miner. Monatsh.* **1978**, 408–421. ICSD 27655.
McMurdie, H., Morris, M., Evans, E., Paretzkin, B., Wong-Ng, W. & Hubbard, C. (1986). *Powder Diffr.* **1**, 86. PDF 36-1484.
Miletich, R., Seifert, F. & Angel, R. J. (1998). *Z. Kristallogr.* **213**, 288–295.
Mogare, K. M., Friese, K., Klein, W. & Jansen, M. (2004). *Z. Anorg. Allg. Chem.* **630**, 547–552.
Morimoto, N., Akimoto, S., Koto, K. & Tokonami, M. (1970). *Phys. Earth Planet. Inter.* **3**, 161–165.
Morris, A. J., Kennard, C. H. L., Moore, F. H., Smith, G. & Montgomery, H. (1981). *Cryst. Struct. Commun.* **10**, 529–532. ICSD 300021.
Müller-Buschbaum, Hk. (2003). *J. Alloys Comput.* **349**, 49–104.
Mumme, W., Cranswick, L. D. & Chakoumakos, B. (1996). *Neues Jahrb. Miner. Abh.* **170**, 171–188.
Nalbandyan, V. B. (1986). *IV All-Union Meeting on Crystal Chemistry of Inorganic and Coordination Compounds*, Bukhara, pp. 213–214. Moscow: Nauka (in Russian).
Nalbandyan, V. B., Avdeev, M. & Pospelov, A. (2006). *Solid State Sci.* **8**, 1430–1437.
Nalbandyan, V. B., Belyaev, I. N., Lupeiko, T. G. & Mezhzhorina, N. V. (1979). *Zh. Neorg. Khim.* **24**, 1546–1552 (in Russian).
Nalbandyan, V. B., Medvedeva, L. I. & Ivleva, T. I. (1995). *Russ. J. Inorg. Chem.* **40**, 719–723.
Nalbandyan, V. B. & Shukaev, I. L. (1987). *Russ. J. Inorg. Chem.* **32**, 453.
Natl. Bur. Stand. (U.S.) (1957). *Circ.* **539**, 7, 45. PDF 8-473.
Natl. Bur. Stand. (U.S.) (1960). *Circ.* **539**, 10, 13. PDF 10-83.
Natl. Bur. Stand. (U.S.) (1968). *Monogr.* **25**, 6, 48. PDF 20-926.
Navrotsky, A. (1971). *J. Inorg. Nucl. Chem.* **33**, 4035–4050.
Navrotsky, A. (1973). *J. Solid State Chem.* **6**, 21–41.
Navrotsky, A. (1980). *CALPHAD*, **4**, 255–264.
Navrotsky, A. (1987). *Prog. Solid State Chem.* **17**, 53–86.
Nimmo, J. K. (1981). *Acta Cryst.* B**37**, 431–433.
Nishi, F. & Takeuchi, Y. (1991). European Crystallographic Meeting 13, 197. PDF 71-5095.
Nishi, F. & Takeuchi, Y. (1996). *Z. Kristallogr.* **211**, 607–611.
Nord, A. G. (1973). *Acta Chem. Scand.* **27**, 814–822.
Nord, A. G. (1976). *Acta Cryst.* B**32**, 982–983.
Nord, A. G. & Werner, P.-E. (1992). *Neues Jahrb. Miner. Monatsh.* pp. 481–486. ICSD 72908.
Okada, K., Morikawa, H., Marumo, F. & Iwai, S. (1974). *Acta Cryst.* B**30**, 1872–1873.
Okada, K. & Ossaka, J. (1980). *Acta Cryst.* B**36**, 919–921.
Okada, K., Ossaka, J. & Iwai, S. (1979). *Acta Cryst.* B**35**, 2189–2191.
O'Keeffe, M. & Brese, N. E. (1991). *J. Am. Chem. Soc.* **113**, 3226–3229.
O'Keeffe, M. & Hyde, B. G. (1985). *Struct. Bond.* **61**, 77–144.
Orosel, D., Balog, P., Liu, H., Qian, J. & Jansen, M. (2005). *J. Solid State Chem.* **178**, 2602–2607.
Palenik, G. J. (1967). *Inorg. Chem.* **6**, 507–511.
Pannetier, G. & Gaultier, G. (1966). *C. R. Acad. Sci.* **263**, 132–134.
Paques-Ledent, M. Th. (1975). *Chem. Phys. Lett.* **35**, 375–378.
Parfitt, D. C., Keen, D. A., Hull, S., Crichton, W. A., Mezouar, M., Wilson, M. & Madden, P. A. (2005). *Phys. Rev. B*, **72**, 054121.
Peskov, M. V. & Blatov, V. A. (2004). *Russ. J. Inorg. Chem.* **49**, 1042–1050.
Peskov, M. V. & Blatov, V. A. (2006). *Russ. J. Inorg. Chem.* **51**, 759–768.
Petit, P. E., Guyot, F., Fiquet, G. & Itie, J. P. (1996). *Phys. Chem. Miner.* **23**, 173–185.
Pistorius, C. W. F. T. (1966). *J. Chem. Phys.* **44**, 4532–4537.
Pistorius, C. W. F. T. (1967*a*). *J. Phys. Chem. Solids*, **28**, 1811–1819.
Pistorius, C. W. F. T. (1967*b*). *J. Chem. Phys.* **46**, 2167–2171.
Pistorius, C. W. F. T. (1967*c*). *J. Phys. Chem. Solids*, **28**, 449–451.
Pistorius, C. W. F. T. (1967*d*). *J. Chem. Phys.* **43**, 2895–2898.
Pistorius, C. W. F. T. & Rapoport, E. (1969). *J. Phys. Chem. Solids*, **30**, 195–201.

Pontonnier, L., Caillet, M. & Aleonard, S. (1972). *Mater. Res. Bull.* **7**, 799–812.
Prewitt, C. T. & Downs, R. T. (1998). *Reviews in Mineralogy, 37, Ultrahigh-Pressure Mineralogy: Physics and Chemistry of the Earth's Deep Interior*, edited by R. J. Hemley, pp. 283–317. Washington: Mineralogical Society of America.
Ravindran, T. R. & Arora, A. K. (1999). *High Pressure Res.*, **16**, 233–242.
Reynard, B., Remy, C. & Takir, F. (1997). *Phys. Chem. Miner.* **24**, 77–84.
Ringwood, A. E. & Reid, A. F. (1968). *Earth Planet. Sci. Lett.* **5**, 67–70.
Ringwood, A. E. & Reid, A. F. (1969). *Earth Planet. Sci. Lett.* **5**, 245–250.
Ringwood, A. E. & Reid, A. F. (1970). *J. Phys. Chem. Solids*, **31**, 279l–2793.
Sato, M. & Kano, S. (1994). *Chem. Lett.* **23**, 427–430.
Shannon, R. D. (1976). *Acta Cryst.* A**32**, 751–767.
Sharma, S. M. & Sikka, S. K. (1995). *Phys. Rev. Lett.* **74**, 3301.
Shigematsu, H., Nomura, K., Nishiyama, K., Tojo, T., Kawaji, H., Atake, T., Kawamura, Y., Miyoshi, T., Matsushita, Y., Tanaka, M. & Mashiyama, H. (2011). *Ferroelectrics*, **414**, 195–200.
Silva, I. da, González-Silgo, C., González-Platas, J., Rodrígues-Carvajal, J., Martínez-Sarrión, M. L. & Mestres, L. (2005*a*). *J. Solid State Chem.* **178**, 1601–1608.
Silva, I. da, González-Silgo, C., González-Platas, J., Rodríguez-Carvajal, J., Martínez-Sarrión, M. L. & Mestres, L. (2005*b*). *Acta Cryst.* C**61**, i113–i116.
Simonov, M. A., Belokoneva, E. L. & Belov, N. V. (1981). *Zh. Strukt. Khim.* **22**, 199–200 (in Russian).
Syono, Y. & Akimoto, S. I. (1971). *J. Solid State Chem.* **3**, 369–380.
Takahashi, I., Onodera, A. & Shiozaki, Y. (1987). *Acta Cryst.* C**43**, 179–182.
Tamada, O., Fujino, K. & Sasaki, S. (1983). *Acta Cryst.* B**39**, 692–697.
Tanaka, K., Naruse, H., Morikawa, H. & Marumo, F. (1991). *Acta Cryst.* B**47**, 581–588.
Vainstein, B. K., Fridkin, V. M. & Indenbom, V. L. (1979). Editors. *Modern Crystallography*, original Russian edition, Vol. 2, pp. 90–91. Moscow: Nauka.
Vegas, A. (2000). *Crystallogr. Rev.* **7**, 189–283.
Vegas, A. (2011). *Struct. Bond.* **138**, 133–198.
Vegas, A. & Jansen, M. (2002). *Acta Cryst.* B**58**, 38–51.
Vegas, Á. & Mattesini, M. (2010). *Acta Cryst.* B**66**, 338–344.
Vereschagin, L. F. & Kabalkina, S. S. (1979). *Rentgenostrukturnye issledovaniya pri vysokom davlenii* (X-ray structural studies at high pressure), pp. 16–19. Moscow: Nauka. (In Russian).
Von Dreele, R. B., Navrotsky, A. & Bowman, A. L. (1977). *Acta Cryst.* B**33**, 2287–2288.
Weber, H. J., Schulz, M., Schmitz, S., Granzin, J. & Siegert, H. (1989). *J. Phys. Condens. Matter*, **1**, 8543–8547.
Weil, M. (2003). *Z. Naturforsch. B*, **58**, 1091–1096.
Welch, M. D., Cooper, M. A. & Hawthorne, F. C. (2001). *Mineral. Mag.* **65**, 441–444.
Yamazaki, S. & Toraya, H. (1999). *J. Appl. Cryst.* **32**, 51–59.
Zachariasen, W. H. (1971). *Kristallografiya*, **16**, 1161–1166.
Zakutkin, Yu. A. & Blatov, V. A. (2001). *J. Struct. Chem.* **42**, 436–445.
Zhang, X. & Zunger, A. (2010). *Adv. Funct. Mater.* **20**, 1944–1952.
Zúñiga, F. J., Breczewski, T. & Arnaiz, A. (1991). *Acta Cryst.* C**47**, 638–640.